Stem Cell Reports
Article

ISSCR

OPEN ACCESS

The role of *UBE3A* in the autism and epilepsy-related Dup15q syndrome using patient-derived, CRISPR-corrected neurons

Marwa Elamin,[1] Aurelie Dumarchey,[2] Christopher Stoddard,[2] Tiwanna M. Robinson,[1] Christopher Cowie,[1] Dea Gorka,[2] Stormy J. Chamberlain,[2] and Eric S. Levine[1,*]

[1]Department of Neuroscience, University of Connecticut School of Medicine, Farmington, CT, USA
[2]Department of Genetics and Genome Sciences, University of Connecticut School of Medicine, Farmington, CT, USA
*Correspondence: eslevine@uchc.edu
https://doi.org/10.1016/j.stemcr.2023.02.002

SUMMARY

Chromosome 15q11-q13 duplication syndrome (Dup15q) is a neurodevelopmental disorder caused by maternal duplications of this region. Autism and epilepsy are key features of Dup15q. *UBE3A*, which encodes an E3 ubiquitin ligase, is likely a major driver of Dup15q because *UBE3A* is the only imprinted gene expressed solely from the maternal allele. Nevertheless, the exact role of *UBE3A* has not been determined. To establish whether *UBE3A* overexpression is required for Dup15q neuronal deficits, we generated an isogenic control line for a Dup15q patient-derived induced pluripotent stem cell line. Dup15q neurons exhibited hyperexcitability compared with control neurons, and this phenotype was generally prevented by normalizing *UBE3A* levels using antisense oligonucleotides. Overexpression of *UBE3A* resulted in a profile similar to that of Dup15q neurons except for synaptic phenotypes. These results indicate that *UBE3A* overexpression is necessary for most Dup15q cellular phenotypes but also suggest a role for other genes in the duplicated region.

INTRODUCTION

Chromosome 15q11-q13 duplication syndrome (Dup15q) is a neurodevelopmental disorder caused by duplications of the 11.2-13.1 region within the long arm of chromosome 15. There are two major genetic subtypes of Dup15q: idic(15), which is caused by an isodicentric supernumerary chromosome that carries two extra copies of the 15q11.2-q13.1 region, and int(15), which arises from a maternal interstitial duplication of the same region. In addition to these two major subtypes, some individuals have a maternal interstitial triplication of 15q11.2-13.1. Autism and seizures are two of the most common behavioral phenotypes of the syndrome (DiStefano et al., 2016). Individuals with Dup15q also present with intellectual disability and substantial fine and gross motor deficits. Clinical studies report that 77%–100% of Dup15q patients are affected by autism (Urraca et al., 2013; Al Ageeli et al., 2014), and 63% of individuals with idic(15) experience seizures, which often present with multiple types and require aggressive treatment with broad-spectrum antiepileptic drugs (Conant et al., 2014). Moreover, epileptic children with Dup15q have an increased risk for sudden unexpected death in epilepsy (SUDEP) (Friedman et al., 2016), therefore, understanding the cellular and molecular mechanisms that lead to seizure generation is of great importance.

In general, two extra maternal copies of 15q11-q13, carried either on an isodicentric extra chromosome or as part of an interstitial triplication, are associated with more severe behavioral, cognitive, and seizure phenotypes compared with maternal interstitial duplications, which have one extra copy of the genetic region (DiStefano et al., 2020). The extra genetic material in Dup15q includes approximately 20 genes (Germain et al., 2014), and active research is devoted toward understanding and identifying the genes that contribute to phenotypes associated with the disorder. Candidate genes include *UBE3A*, which encodes an ubiquitin ligase, *GABRA5*, *GABRB3*, and *GABRG3*, which encode subunits of the $GABA_A$ receptor, *ATP10*, which encodes a mitochondrial inner membrane protein, and *HERC2*, a ubiquitin ligase known to interact with and potentiate *UBE3A* activity (Germain et al., 2014).

Overexpression of *UBE3A* is likely a major driver of Dup15q phenotypes. *UBE3A* encodes an E3 ubiquitin ligase that targets proteins for degradation by the proteasome (Huang et al., 1999). Moreover, it has been reported to act as a transcriptional coactivator for steroid receptors (Nawaz et al., 1999), and it has been implicated in the regulation of multiple genes associated with nervous system development (Low and Chen 2010). *UBE3A* is the only gene in the region expressed solely from the maternal allele, as *UBE3A* is paternally imprinted and silenced in mature neurons; hence, a maternal duplication would increase its gene dosage, whereas a paternal duplication would not (Chamberlain and Lalande 2010). Dup15q is fully penetrant in individuals with maternal duplications, whereas individuals with paternal duplications are usually unaffected or mildly affected (Cook et al., 1997; Urraca et al., 2013), supporting a key role for *UBE3A*. Nevertheless, the contribution of other duplicated genes in the region to Dup15q phenotypes is unknown.

The generation of animal models for Dup15q has been difficult. Creation of an interstitial duplication of the syntenic region in mice resulted in a mouse model with excellent construct validity (Nakatani et al., 2009). However,

this model has poor face validity as there were no behavioral phenotypes with maternal duplication, whereas paternal duplication resulted in subtle autism-like phenotypes (Nakatani et al., 2009). Another study used bacterial artificial chromosome (BAC) transgene to increase the genetic copy number of *Ube3a* from one to three, which resulted in mice with mild autistic behaviors (Smith et al., 2011). Nevertheless, the construct validity of this model came into question, as the C terminal of Ube3a was tagged with a FLAG tag that affected the catalytic function of the protein. Subsequently, the same group created a *Ube3a* overexpression mouse model with untagged Ube3a (Krishnan et al., 2017). These mice had decreased sociability, but only in relation to chemically induced seizures. No spontaneous seizures, altered seizure threshold, or other autism spectrum disorder (ASD)-like phenotypes were observed. A separate group generated a mouse that overexpressed *Ube3a* in excitatory neurons (Copping et al., 2017). This model showed learning disabilities, anxiety-like behavior, and a reduction in seizure threshold. Interestingly, another recent study using a BAC transgene to increase copy number found that *Ube3a*-overexpressing mice were indistinguishable from wild-type controls on a number of molecular and behavioral measures (Punt et al., 2022). Although these models might be valid for studying the cellular and behavioral effects of *Ube3a* overexpression, they fail to encompass the full range of severe Dup15q phenotypes and replicate the complex genetics of the disease. Hence, the use of induced pluripotent stem cell (iPSC)-derived neurons from Dup15q patients represents an excellent first step to study the cellular mechanisms of the disease and identify the relevant genes that contribute to the disease phenotypes.

The goal of this study was to determine the role of *UBE3A* overexpression in Dup15q neuronal phenotypes. We used an innovative approach to generate an isogenic control line for an idic(15) patient-derived iPSC line. Using these lines, we normalized *UBE3A* levels with antisense oligonucleotides (ASOs) in Dup15q neurons to determine whether *UBE3A* overexpression is necessary for establishing cellular phenotypes. To explore whether *UBE3A* overexpression was sufficient to cause Dup15q cellular phenotypes, we differentiated neurons from an iPSC line derived from an individual with a paternal interstitial duplication. We then used ASOs to knockdown the antisense transcript responsible for silencing *UBE3A*, thereby increasing *UBE3A* expression.

RESULTS

Elimination of the isodicentric chromosome 15

We previously showed that patient-derived iPSCs carry the exact genetic makeup of individuals affected by Dup15q and maintain their methylation imprint following the reprogramming process (Germain et al., 2014). In a subsequent study (comparing multiple patient-derived Dup15q and control iPSC lines), we uncovered several hyperexcitability phenotypes in Dup15q neurons, including increased excitatory synaptic event frequency and amplitude and increased action potential (AP) firing (Fink et al., 2021). Although comparisons that involve unrelated control and disease lines provide important and relevant information, inherent functional differences between cell lines (which are likely driven by different genetic backgrounds) can obscure important cellular phenotypes. The use of isogenic cell lines provides a better approach to investigate cellular deficits in disease models, and the development of the CRISPR-Cas9 gene-editing technology has greatly enabled this process, especially for monogenic diseases (Wang et al., 2013; Xiao et al., 2013; Gupta et al., 2018).

We sought to generate an isogenic control for a Dup15q idic(15) patient-derived iPSC line to more confidently ascribe Dup15q cellular phenotypes to the extra genetic material on the idic(15) chromosome. We used a strategy previously used to eliminate chromosome 21 in a trisomy 21 cellular model and the Y chromosome in typical male iPSCs (Adikusuma et al., 2017; Zuo et al., 2017). This strategy entailed the use of CRISPRs to cut multiple times within chromosome 15q-specific repeats. We nucleofected Dup15q iPSCs with a cocktail of three different CRISPRs targeting *GOLGA8*, *SNORD116*, and *SNORD115* (Table S1). The guide RNAs designed to target these loci are each predicted to cut multiple times within chromosome 15q11.2-q13.3 region but are not found outside of the chromosome. Our rationale was that these CRISPRs would make multiple double-stranded breaks on the two chromosomes 15 as well as the supernumerary idic(15) in the iPSC line. As the idic(15) has two copies of 15q11.2-q13.3 and very little additional sequence, we reasoned that the entire chromosome might be lost upon becoming "shredded" by the CRISPR cocktail. Following transient selection for the CRISPRs, clones were screened using quantitative copy number assays for *UBE3A* and *PML*. Idic(15) iPSCs have four copies of *UBE3A*, but only two copies of *PML*, which is located near the distal end of chromosome 15. A total of 58 clones were screened. Representative colonies with a copy number decrease in *UBE3A* and no decrease in PML copy number are shown in Figure S1.

Four clones with reduced *UBE3A* dosage were expanded and subjected to quantitative DNA methylation analysis at the *SNRPN* locus. Clones that had lost the idic(15) chromosome would have 50% methylation at *SNRPN* because of the presence of one maternal and one paternal chromosome 15. Deletions that included the imprinted domain of maternal chromosome 15 or paternal chromosome 15 would have 66% and 100% methylation at *SNRPN*,

respectively. Following this screening paradigm, one single clone from a starting pool of 58 was identified with the appropriate copy number and DNA methylation parameters (Figure 1A). CytoSNP and karyotype analysis confirmed the loss of the idic(15) chromosome without any other detectable copy number changes or structural rearrangements (Figure 1B; Table S2). The presence of non-chromosome 15 copy number changes in the edited iPSCs that were also present in the idic-1 iPSC line confirmed that the cytoSNP profiles and karyotypes of these two cell lines were identical to each other, except for the 15q copy number changes and supernumerary chromosome (Table S2). Finally, qRT-PCR demonstrated that gene expression of imprinted and non-imprinted genes in the 15q region was reduced in the corrected control line compared with idic-1 and very similar to expression levels in unaffected control iPSCs (Figure 1C).

Hyperexcitability of Dup15q neurons during *in vitro* development

To characterize the electrophysiological properties of Dup15q neurons, the idic-1 cell line and its CRISPR-corrected isogenic counterpart were differentiated into neurons using a modified dual-SMAD inhibition protocol (Figure S2A). Differentiation via this protocol yielded neuronal cultures that consisted of neurons expressing the glutamatergic marker TBR1 (70%–80% of MAP2-positive cells) and GABAergic neurons expressing GAD65, as well as astrocytes expressing S100β (Germain et al., 2014; Fink et al., 2021). Immunostaining was carried at 19 weeks *in vitro* to evaluate the differentiation capacity of the iPSC lines. The proportion of MAP2-positive cells was similar for Dup15q and control cultures (Figure S2B).

Whole-cell patch-clamp recordings were conducted at 8 and 19 weeks of *in vitro* development. Dup15q neurons showed a significantly greater inward sodium current density compared with the corrected line at both time points, whereas the transient outward potassium current density was significantly increased at 19 weeks (Figure 2A). Dup15q neurons also showed a significant decrease in input resistance at both time points (Figure 2A). Consistent with the increased inward and outward currents, Dup15q neurons had an increased AP amplitude and decreased AP width (Figure 2B). Increased frequency of induced AP firing and a hyperpolarized AP threshold were also observed in Dup15q neurons at both time points (Figure 2C). Dup15q neurons showed normal maturation of the resting membrane potential (RMP) compared with their corrected counterparts and no difference in cell capacitance (Figures S2C and S2D). Electrophysiological phenotypes in Dup15q neurons were not due to failure of maturation in the corrected line, as the corrected neurons were functionally comparable with neurons derived from an independent healthy control iPSC line (Figure S3).

Altered synaptic transmission and spontaneous firing in Dup15q neurons

Voltage-clamp recordings of Dup15q neurons and corrected isogenic controls revealed a significant increase in the frequency and amplitude of spontaneous excitatory postsynaptic currents (sEPSCs) at 19 weeks (Figure 3A), similar to our previous study comparing Dup15q lines with unaffected controls (Fink et al., 2021). There was also a decrease in the frequency, but not amplitude, of spontaneous inhibitory postsynaptic currents (sIPSCs; Figure 3B). Spontaneous postsynaptic currents consisted of both miniature postsynaptic currents (mPSCs) and AP-dependent currents. To isolate AP-independent miniature synaptic events, a separate series of recordings were carried out in the presence of 1 μM tetrodotoxin (TTX). Dup15q neurons showed an increase in miniature excitatory postsynaptic current (mEPSC) frequency and amplitude (Figure 3C). There were no significant differences in miniature inhibitory postsynaptic currents (mIPSCs) (Figure 3D). The increase in mEPSC frequency may reflect increased synapse number and/or increased presynaptic release probability. Immunostaining for the postsynaptic marker PSD95, however, failed to detect an increase in the density of PSD95 puncta in Dup15q neurons (Figure 3E). The increased sEPSC amplitude may also reflect an increase in spontaneous neuronal firing, as AP-dependent events are associated with higher amplitudes compared with miniature synaptic events. Supporting this, there was a significant increase in the number of AP-dependent calcium transients in Dup15q neurons (Figure 3F).

The contribution of *UBE3A* overexpression to Dup15q cellular phenotypes

UBE3A is exclusively expressed from the maternal allele in mature neurons, thus overexpression of this gene is thought to be a critical factor in the development of the maternally inherited syndrome. To examine the contribution of *UBE3A* to Dup15q cellular phenotypes, we normalized expression in idic(15) Dup15q neurons using ASOs targeting *UBE3A*. ASOs bind to RNA in a sequence-specific manner and recruit RNAse H to cleave the RNA bound to the DNA-like core of the ASO (DeVos and Miller 2013; Meng et al., 2015). This, in turn, recruits exonucleases leading to the knockdown of the target RNA. Intriguingly, ASOs are freely taken up by neurons without the use of transfection reagents, allowing the knockdown of the intended genes in every neuron within the culture (Meng et al., 2015). Furthermore, ASO effects are concentration dependent and highly stable, with a single treatment leading to enduring knockdown in post-mitotic

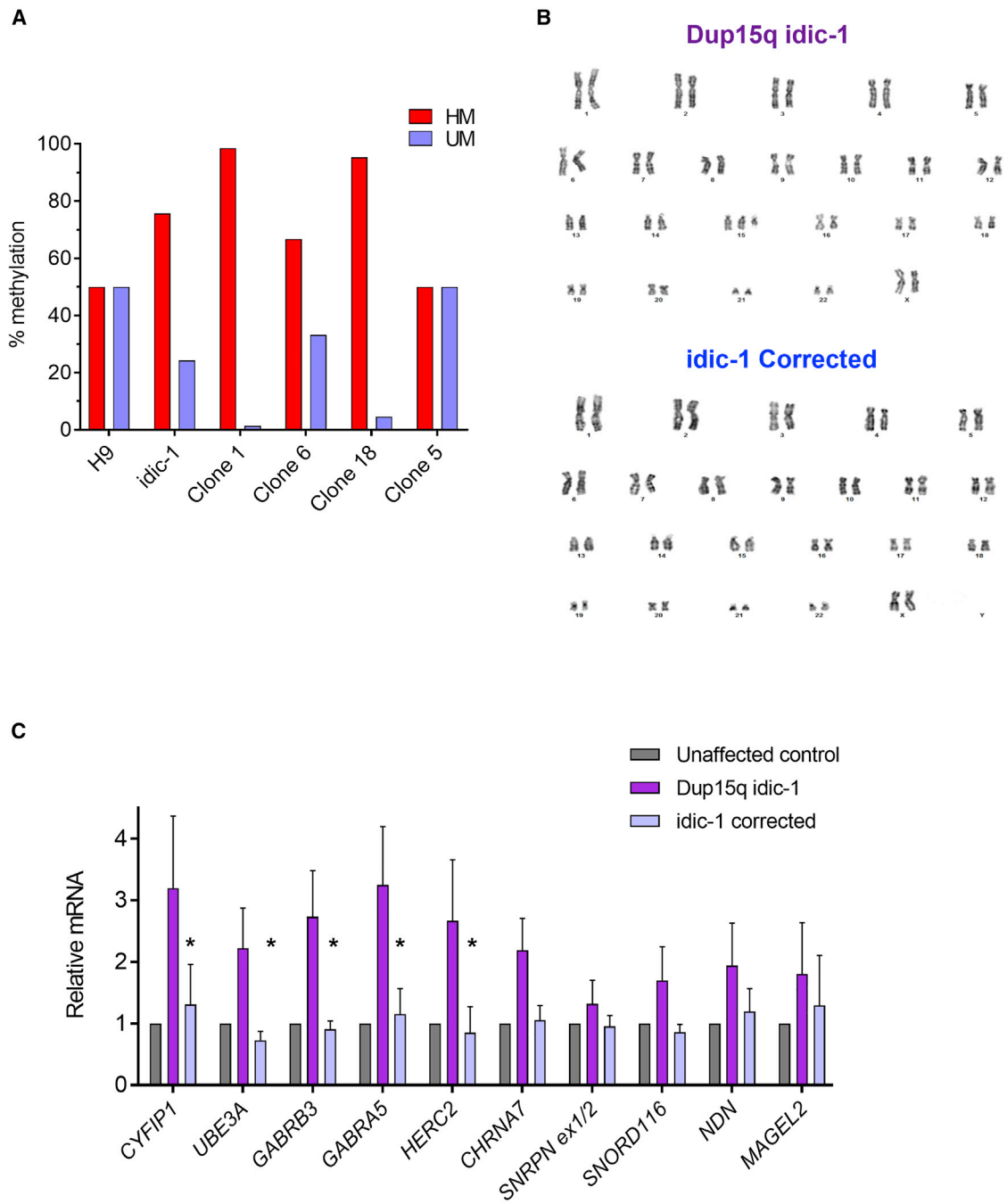

Figure 1. Generation of Dup15q isogenic corrected iPSC line

(A) Methylation status of clones compared with idic-1 Dup15q parent line and H9 control line. HM, hypermethylated; UM, unmethylated.

(B) Karyotyping of idic-1 iPSC line (top) and corrected clone 5 of idic-1 (bottom). Note the loss of the idic(15) chromosome.

(C) qRT-PCR analysis of maternally expressed genes (*UBE3A*), non-imprinted genes (*CYFIP1*, *GABRB3*, *GABRA5*, *HERC2*, and *CHRNA7*), and paternally expressed genes (*SNRPN*, *SNORD116*, *NDN*, and *MAGEL2*) in the 15q locus in idic-1 iPSCs and the corrected idic-1 line (n = 4 biological replicates). RNA levels are presented relative to an unaffected control iPSC line. Statistical analysis compared idic-1 corrected with Dup15q idic-1. *$p < 0.05$ (Student's t test).

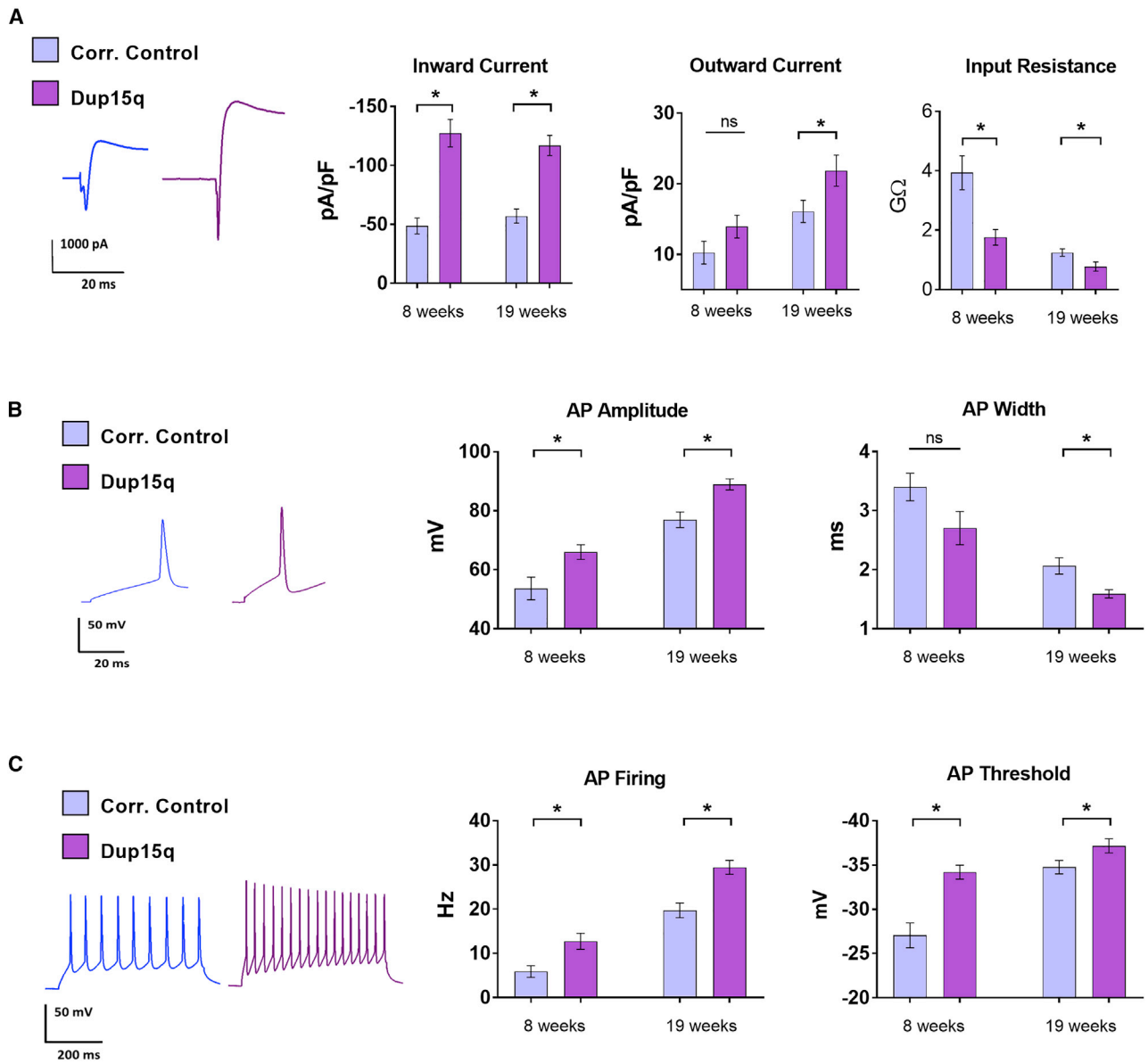

Figure 2. Cellular phenotypes of idic(15) Dup15q neurons compared with isogenic corrected control

(A) Left: example traces of inward and outward currents elicited with a voltage step from −70 to +40 mV at 19 weeks of *in vitro* development. Middle: maximum inward and outward current density. Right: input resistance.

(B) Left: example action potential (AP) traces elicited by +80 pA current step. Middle: peak AP amplitude. Right: AP width at half-maximal amplitude.

(C) Left: AP traces during a 500 ms current step elicited by +80 pA. Middle: maximum AP firing rate. Right: AP threshold. n = 22–25 cells per group from 2 independent differentiations. *p < 0.05 (Student's t test).

neurons (Meng et al., 2015). We have previously designed and characterized ASOs that selectively reduce the expression of *UBE3A* with high efficiency, resulting in immediate, and long-lasting, knockdown of both mRNA and protein levels (Fink et al., 2017). To normalize *UBE3A* levels in Dup15q neurons, ASO treatment (10 μM) was initiated at two time points: at 6 weeks *in vitro*, to identify a role of *UBE3A* in the establishment of cellular phenotypes, and at 16 weeks, to determine if established phenotypes can be reversed. Patch-clamp recordings were performed at week 19 (Figure 4A). Neurons were collected 2–3 weeks post-treatment and the level of

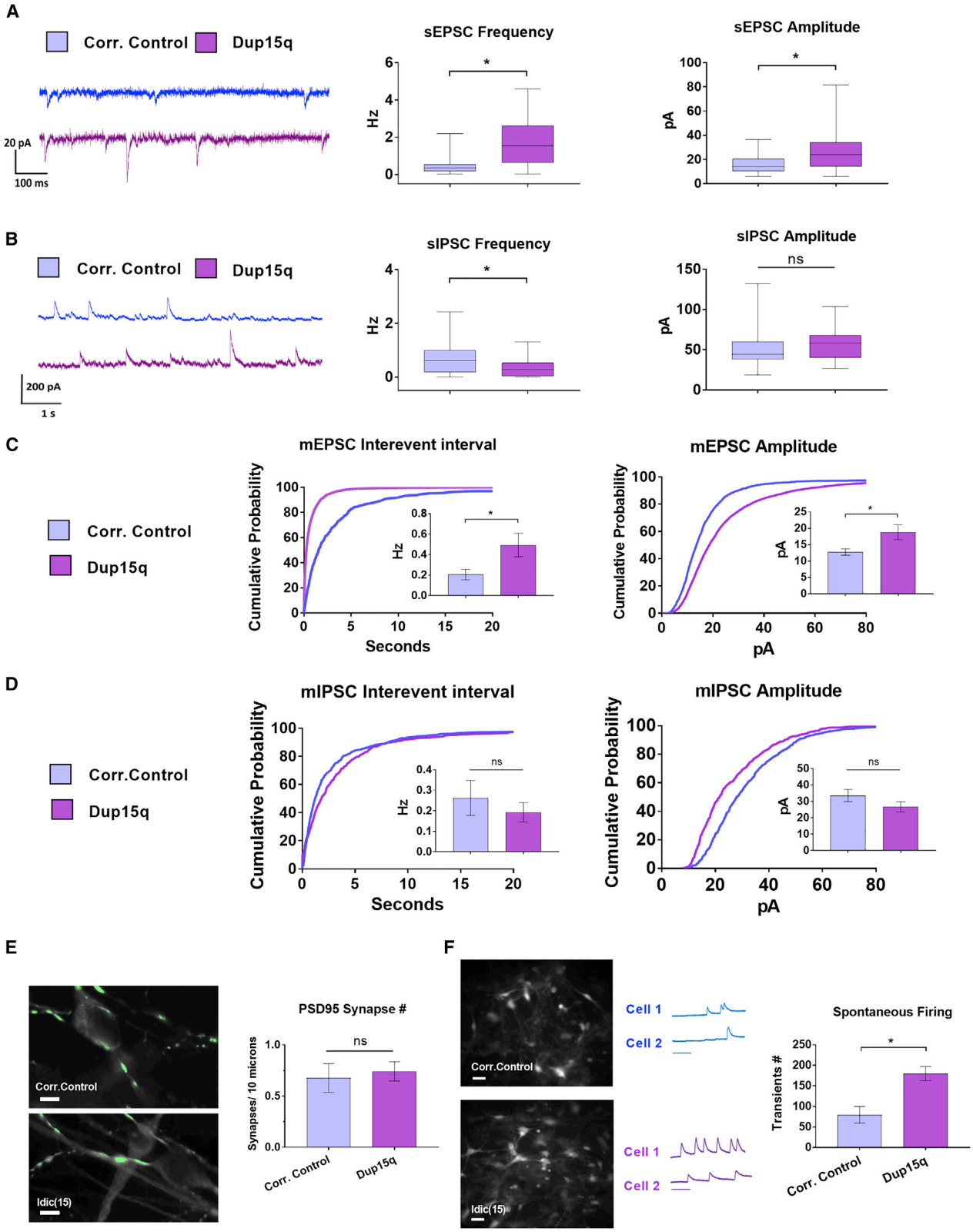

(legend on next page)

UBE3A mRNA was confirmed via qRT-PCR (Figure 4B). A scrambled sequence ASO was used to control for non-specific effects.

Normalizing *UBE3A* expression at 6 weeks prevented the increased inward and outward currents (Figures 4C and 4D), the increased AP amplitude (Figure 4E), the decreased AP width (Figure 4F), the increased AP firing rate (Figure 4G), and the hyperpolarized AP threshold (Figure 4H) when recordings were carried out at 19 weeks. Interestingly, *UBE3A* normalization failed to reverse changes in input resistance (Figure 4I). *UBE3A* normalization at 16 weeks failed to reverse these phenotypes at 19 weeks (Figures 4C–4H). To determine if normalizing *UBE3A* at 6 weeks prevented the expression of these phenotypes within 2 weeks of treatment, we performed patch-clamp recordings in 8-week-old neurons after treatment with *UBE3A* ASO at 6 weeks. The increase in inward current was completely normalized at 8 weeks (Figure S4A). A similar trend was seen in outward current, AP firing rate, amplitude, and threshold, although not statistically significant (Figures S4B–S4D). To determine if ASO treatment had non-specific effects on electrophysiological parameters, we compared scramble ASO-treated cells to untreated cells and found no differences between the two groups (Figure S5). To confirm the role of *UBE3A* in the aforementioned phenotypes, we normalized *UBE3A* levels in a different Dup15q line with the same genetic aneuploidy (idic-2). Normalization of *UBE3A* levels at 6 weeks decreased inward current, outward current, AP amplitude, and AP firing rate (Figure S6). In summary, *UBE3A* normalization at 6 weeks prevented the development of neuronal hyperexcitability, indicating that *UBE3A* overexpression is necessary for the development of these cellular phenotypes.

To investigate the contribution of *UBE3A* to the synaptic phenotypes in Dup15q neurons, we used ASOs to normalize *UBE3A* levels starting at either 6 or 16 weeks of *in vitro* development and recorded synaptic activity at 19 weeks. *UBE3A* normalization at 6 weeks prevented the increased sEPSC frequency and amplitude in Dup15q neurons, whereas treatment at 16 weeks failed to do so (Figure 5A). Interestingly, normalization of *UBE3A* levels at both time points normalized the decrease in sIPSC frequency (Figure 5B). *UBE3A* ASO treatments at both 6 and 16 weeks were only partially effective in normalizing the increase in mEPSC frequency (Figure 5C; differences are not statistically significant), although mEPSC amplitude was corrected by ASO treatment at 6 weeks (Figure 5C). Moreover, normalizing *UBE3A* levels did not have a significant effect on mIPSC frequency or amplitude (Figure 5D). To test if the *UBE3A* effect on spontaneous excitatory events is partially caused by changes in spontaneous AP firing, we performed population calcium imaging experiments. Normalizing *UBE3A* at either 6 or 16 weeks reduced the spontaneous frequency of calcium transients in Dup15q neurons (Figure 5E). These findings suggest that *UBE3A* is necessary for the development of the increased spontaneous excitatory transmission and spontaneous neuronal firing in Dup15q cells. Although normalization of *UBE3A* level at 16 weeks was less effective in reversing some phenotypes compared with treatment at 6 weeks, it successfully normalized the deficit in spontaneous inhibitory transmission (Figure 5B) and the increase in spontaneous neuronal firing (Figure 5E).

Figure 3. Synaptic transmission and spontaneous firing in Dup15q neurons

(A) Left: example sweeps of spontaneous excitatory postsynaptic currents (sEPSCs) at 19 weeks. Cells were voltage clamped at −70 mV. Middle: sEPSC frequency at 19 weeks. Right: sEPSC amplitude at 19 weeks. Box-and-whisker plots represent the first quartile, median, and third quartile; bars represent 2.5th to 97.5th percentile outliers (n = 22–25 cells per group from 2 independent differentiations). *p < 0.05 (Mann-Whitney U test).

(B) Left: example sweeps of spontaneous inhibitory postsynaptic currents (sIPSCs) at 19 weeks. Cells were held at 0 mV. Middle: sIPSC frequency at 19 weeks. Right: sIPSC amplitude at 19 weeks. Box-and-whisker plots as above (n = 22–25 cells per group from 2 independent differentiations).

(C) Miniature excitatory postsynaptic currents (mEPSCs) recorded at −70 mV in the presence of 1 μM TTX. Left: cumulative probability histogram of the interevent interval of all mEPSC events. Inset: frequency of mEPSC per cell, represented as mean ± SEM. Right: cumulative probability histogram of the amplitude of all mEPSC events. Inset: amplitude of mEPSC per cell, represented as mean ± SEM (n > 20 cells per group). *p < 0.05 (unpaired t tests).

(D) Miniature inhibitory postsynaptic currents (mIPSCs) recorded at −70 mV in the presence of 1 μM TTX. Left: interevent interval of all mEPSC events recorded across all cells. Inset: frequency of mIPSCs per cell. Right: cumulative probability histogram of the amplitude of all mIPSC events recorded across all cells. Inset: amplitude of mIPSC per cell (n = 15 cells in each group from 2 independent differentiations). *p < 0.05 (Student's t test).

(E) Representative images of PSD95 immunostaining and density of PSD95 puncta in 19-week-old neurons (n = 10 coverslips per group from 2 separate differentiations, unpaired t test). Scale bar: 10 μm.

(F) Calcium imaging. Left: representative images of Dup15q and corrected neurons after incubation with X-Rhod-1 fluorescent dye. Scale bar: 50 μm. Middle: example traces of spontaneous calcium transients. Scale bar: 100 s. Right: number of spontaneous calcium transients per coverslip over 15 min (n = 5 coverslips per group from 2 independent differentiations). *p < 0.05 (unpaired t test).

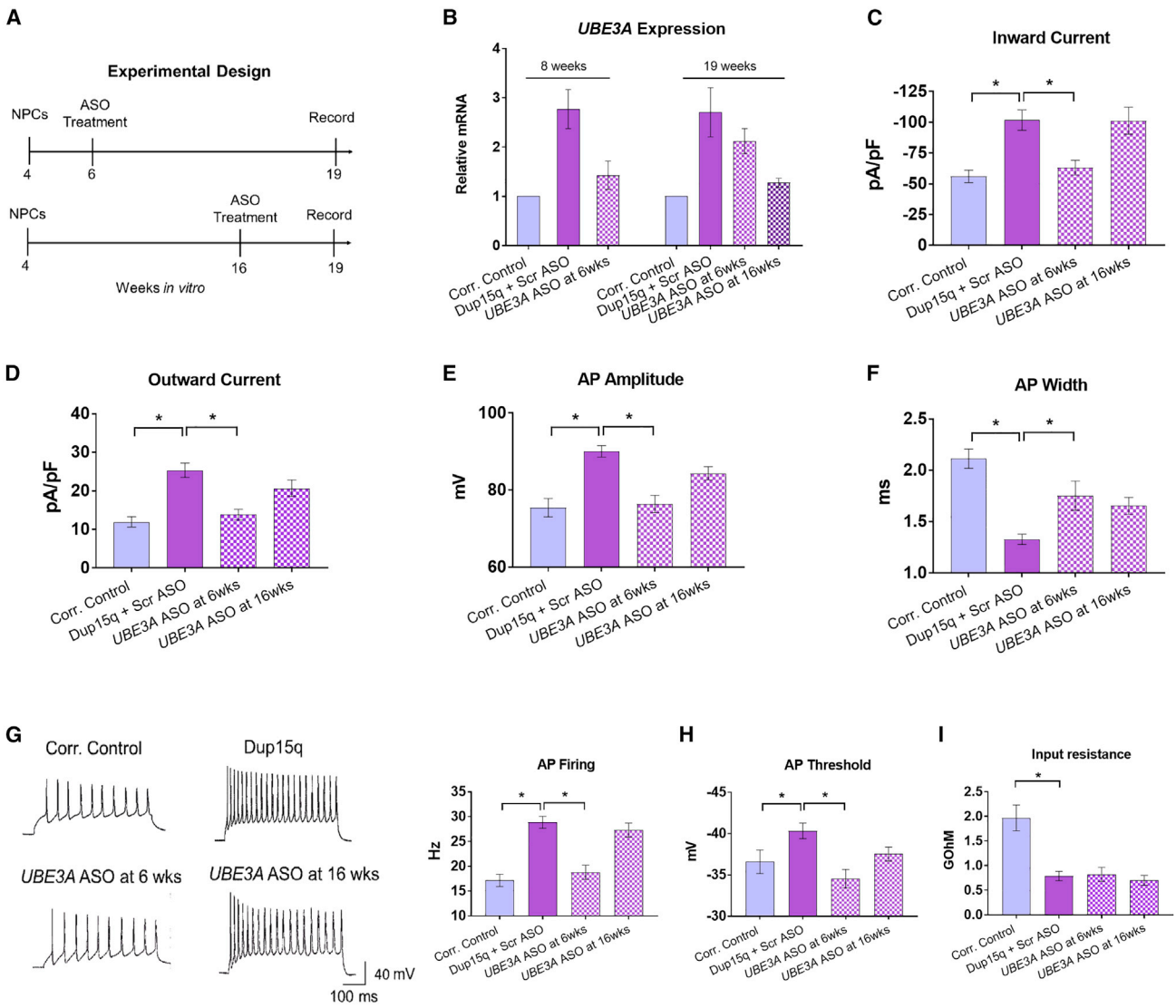

Figure 4. Normalization of *UBE3A* expression prevents intrinsic phenotypes in Dup15q neurons

(A) Experimental design of *UBE3A* ASO treatments and recording times.

(B) Relative expression of *UBE3A* mRNA in corrected control neurons and Dup15q neurons treated with either scramble (Scr) ASO or *UBE3A* ASO. For gene expression at 8 weeks, neurons were treated with ASOs at 6 weeks. For gene expression at 19 weeks, neurons were treated with ASOs either at 6 weeks or at 16 weeks (n = 2 biological replicates).

(C) Maximum inward current density.

(D) Maximum outward current density.

(E) Action potential (AP) amplitude.

(F) AP width.

(G) Left: representative traces of AP firing at 19 weeks during a 500 ms current step from −10 to +80 pA. Right: AP firing rate.

(H) AP threshold.

(I) Input resistance (n = 22–30 cells per group from 2 independent differentiations). *p < 0.05 (one-way ANOVA and Dunnett's multiple-comparisons tests).

UBE3A overexpression recapitulates key cellular phenotypes in Dup15q neurons

To study the consequences of *UBE3A* overexpression in the context of other duplicated genes in the region, and to confirm that the observed intrinsic excitability and synaptic phenotypes are modulated by *UBE3A*, we increased *UBE3A* dosage in an iPSC line with a paternal duplication (PatDup) in BP2-BP3 of the 11.2-13.1 region of chromosome

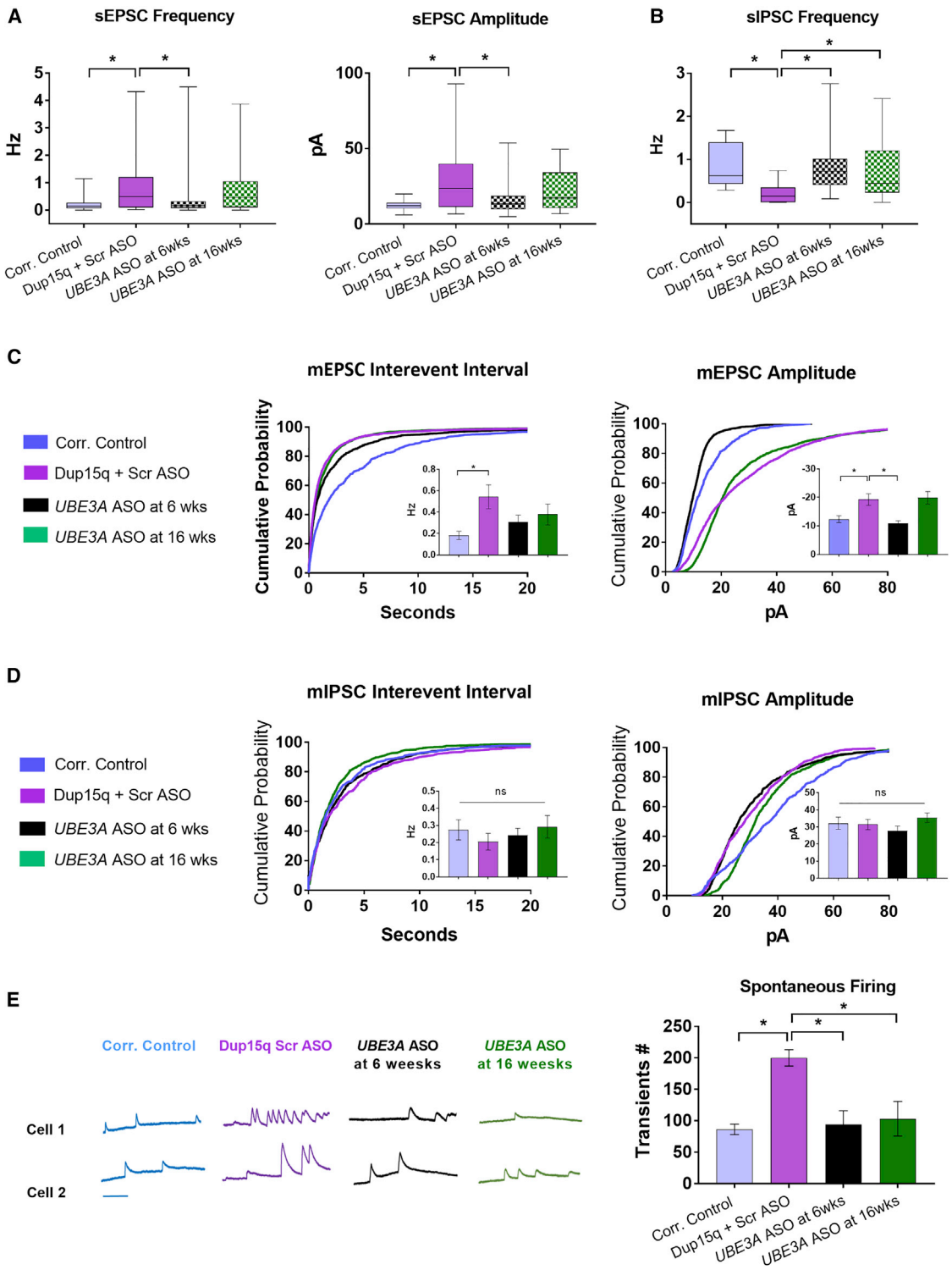

Figure 5. Normalization of *UBE3A* affects synaptic transmission and spontaneous firing phenotypes in Dup15q neurons

(A) Frequency (left) and amplitude (right) of spontaneous excitatory postsynaptic currents (sEPSCs) in corrected neurons, Dup15q neurons treated with 10 μM scramble ASO, Dup15q neurons treated with 10 μM *UBE3A* ASO at 6 weeks, and Dup15q neurons treated with 10 μM *UBE3A* ASO at 16 weeks (n = 22–32 cells per group from 2 independent differentiations).

(B) Frequency of spontaneous inhibitory postsynaptic currents (sIPSCs) in corrected neurons, Dup15q neurons treated with 10 μM scramble ASO, Dup15q neurons treated with *UBE3A* ASO at 6 weeks, and Dup15q neurons treated with *UBE3A* ASO at 16 weeks (n = 22–32

(legend continued on next page)

15. This line, which contains two silenced copies of *UBE3A*, was previously characterized and does not display Dup15q cellular phenotypes (Fink et al., 2021). *UBE3A* overexpression was achieved by using ASOs targeting *UBE3A-ATS*, a non-coding RNA that silences the paternal copy of *UBE3A*. These *ATS*-ASOs would theoretically increase *UBE3A* gene dosage from one active copy to three active copies, mimicking the expression level in idic(15) Dup15q syndrome. These cells also have one extra copy of the non-imprinted genes in the 15q11.2-q13 region. We previously confirmed the ability of this specific ASO to reduce *UBE3A-ATS*, leading to a long-lasting increase (for a minimum of seven weeks) in *UBE3A* mRNA and protein levels (Germain et al., 2021).

To determine if early overexpression of *UBE3A* causes the same electrophysiological phenotypes that were observed in Dup15q neurons, *ATS* ASOs and scramble ASOs (10 μM) were applied to PatDup cells at 6 weeks of *in vitro* development (experimental design; Figure 6A). *UBE3A mRNA* was quantified via qRT-PCR and found to be approximately twice the level of *UBE3A* found in scramble ASO-treated PatDup neurons (Figure 6B). Patch-clamp recordings performed at 19 weeks revealed that *UBE3A* overexpression resulted in a hyperexcitability profile similar to that of Dup15q neurons. Specifically, a significant increase in inward current, an increase in AP amplitude, an increase in AP firing frequency, and a hyperpolarized AP threshold were observed (Figures 6D–6G). Nevertheless, not all phenotypes were recapitulated by *UBE3A* overexpression. Except for an increase in sIPSC amplitude, neither excitatory nor inhibitory synaptic activity was altered upon *UBE3A* overexpression in PatDup neurons (Figures 6H and 6I), nor was input resistance (Figure 6C).

DISCUSSION

Maternal duplications in the 11.2-13.1 region of chromosome 15 cause Dup15q syndrome, a disorder characterized by autism, epileptic seizures, and a wide range of intellectual and motor disabilities (Kalsner and Chamberlain 2015; DiStefano et al., 2016). The parent of origin is important for Dup15q because maternal duplications cause the syndrome, while individuals with a paternal duplication typically display a normal phenotype (Cook et al., 1997; Hogart et al., 2010; Aypar et al., 2014), although developmental abnormalities have also been associated with paternal duplications (Mohandas et al., 1999; Mao et al., 2000; Marini et al., 2013). It is thought that *UBE3A*, the gene encoding the ubiquitin protein ligase E3A, plays a critical role in Dup15q phenotypes because it is the only imprinted gene that is expressed solely from the maternal allele in neurons. Animal models of *UBE3A* overexpression have been used to study the syndrome, but with limited success in recapitulating the full range of Dup15q phenotypes (Smith et al., 2011; Copping et al., 2017). Maternal duplication of the syntenic mouse region also failed to replicate behavioral and physiological phenotypes (Nakatani et al., 2009), thus, fundamental knowledge regarding the cellular mechanisms of Dup15q and the role of *UBE3A* in the development of the syndrome is lacking.

Here, we used an innovative CRISPR strategy to successfully eliminate the extra chromosome in an idic(15) Dup15q human iPSC line, thereby creating an isogenic control line. We used these lines to determine the functional differences between Dup15q and corrected neurons and investigate the role of *UBE3A* in Dup15q cellular phenotypes. Dup15q neurons exhibited multiple hyperexcitability phenotypes compared with isogenic corrected control neurons, which include increased AP firing, increased frequency of excitatory synaptic currents, and decreased frequency of inhibitory current, changes consistent with our previous findings (Fink et al., 2021). Moreover, the isogenic comparison in this study uncovered differences in inward current, AP amplitude, and input resistance that were not observed in our previous study comparing patient lines to unaffected control lines. The differentiation protocol used in this study generates multiple cell types, but the majority are glutamatergic excitatory neurons. It is worth noting that, in Angelman syndrome

cells per group from 2 independent differentiations). Box-and-whisker plots represent the first quartile, median, and third quartile; bars represent 2.5th to 97.5th percentile outliers. *p < 0.05 (non-parametric Mann-Whitney U test).

(C) Left: cumulative probability histogram of the interevent interval of all mEPSC events across all cells. Inset: frequency of mEPSC per cell, represented as mean ± SEM. Right: cumulative probability histogram of the amplitude of all mEPSC events across all cells. Inset: amplitude of mEPSC per cell, represented as mean ± SEM (n = 20–29 cells per group from 2 independent differentiations). One-way ANOVA and Dunnett's multiple-comparisons tests.

(D) Left: cumulative probability histogram of the interevent interval of all mIPSC events across all cells. Inset: frequency of mIPSC per cell, represented as mean ± SEM. Right: cumulative probability histogram of the amplitude of all mIPSC events across all cells. Inset: amplitude of mIPSCs per cell (n = 15 or 16 cells per group from 2 independent differentiations). One-way ANOVA and Dunnett's multiple-comparisons tests.

(E) Calcium imaging. Left: example traces of spontaneous calcium transients in two different cells per group. Right: number of spontaneous calcium transient per coverslip over 15 min (n = 5 coverslips per group from 2 independent differentiations). Scale bar: 100 s. *p < 0.05 (one-way ANOVA and Dunnett's multiple-comparisons tests).

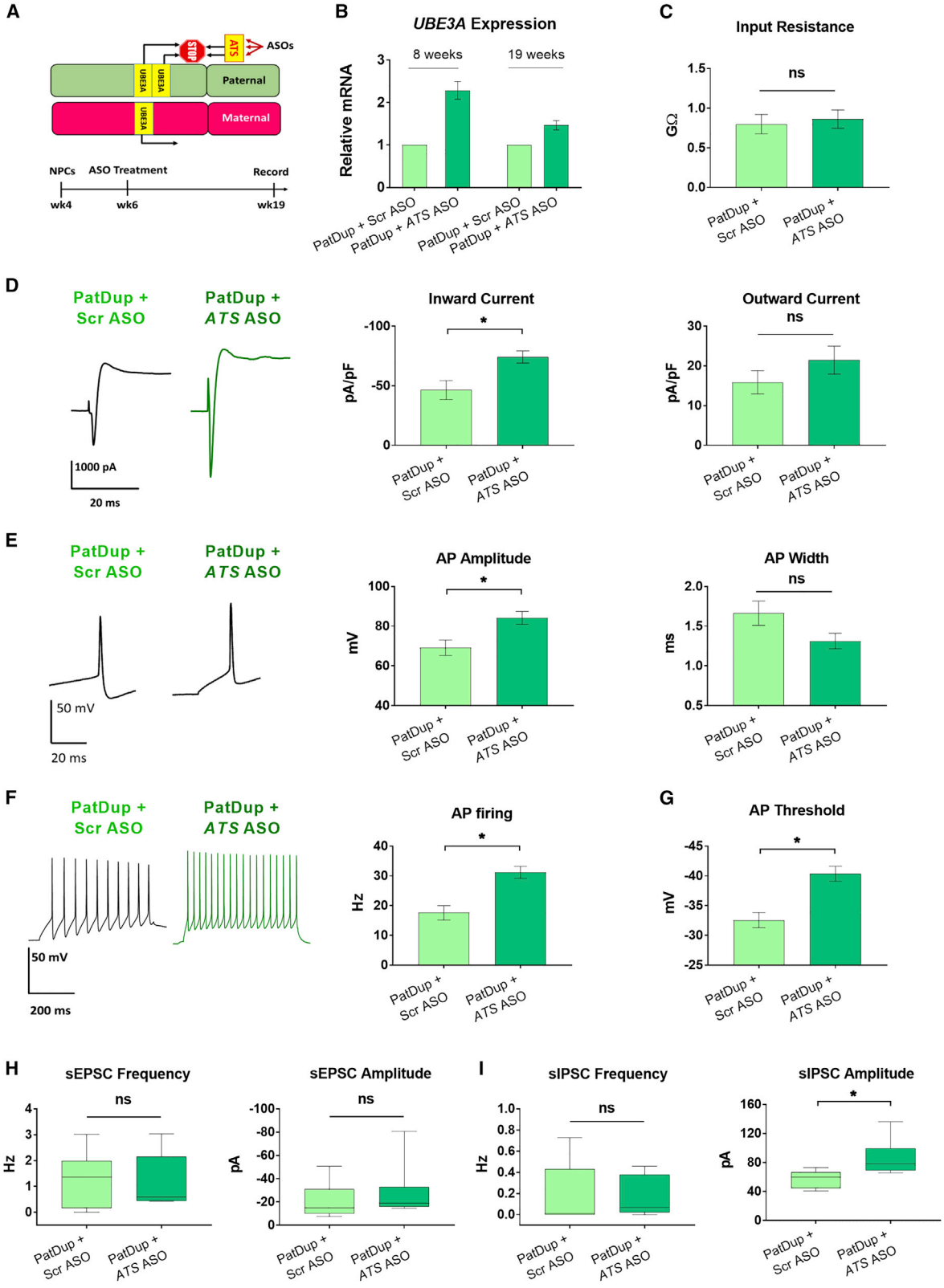

(legend on next page)

model mice, the loss of *UBE3A* in GABAergic neurons has been shown to be a principal cause of circuit hyperexcitability (Judson et al., 2016), thus it will be important in future studies to explore the specific contribution of *UBE3A* overexpression in inhibitory neurons to changes in network activity in Dup15q.

One critical question for Dup15q is whether a single gene drives the cellular and patient phenotypes. Our data demonstrated that most Dup15q neuronal phenotypes were prevented by normalizing *UBE3A* levels, indicating that excess *UBE3A* is necessary for their development. The majority of idic(15) Dup15q cellular phenotypes were also recapitulated by overexpressing *UBE3A* in PatDup neurons, further supporting a role for excess *UBE3A* in their establishment. Both of these conditions evaluated excess *UBE3A* in the context of duplicated non-imprinted genes. That is, excess *UBE3A* plus excess *GABRB3*, *GABRA5*, *GABRG3*, *HERC2*, and other genes. It is still unknown whether *UBE3A* overexpression alone is sufficient to cause these phenotypes. For instance, deficits in excitatory and inhibitory transmission and input resistance in Dup15q neurons were not replicated by *UBE3A* overexpression in PatDup neurons, nor fully corrected by normalizing *UBE3A* level in Dup15q neurons. These results support a role for other non-imprinted duplicated genes in the development of these deficits, and suggest that one extra copy of the non-imprinted genes in the PatDup neurons may be insufficient to replicate the synaptic and input resistance phenotypes seen in idic Dup15q neurons that have 2 extra copies of the non-imprinted genes. Nonetheless, even if duplication of the non-imprinted genes contributes to the cellular phenotypes, our data suggest that normalization of *UBE3A* alone may ameliorate the majority of neuronal phenotypes in our human *in vitro* model system. This suggests that therapeutics that target *UBE3A* might influence neuronal excitability and potentially alter the disease course of individuals with Dup15q.

Normalizing *UBE3A* expression at 16 weeks failed to fully reverse many phenotypes in our experimental paradigm. It is possible that a longer treatment time may be required to reverse these phenotypes in mature neurons, or that optimal connectivity achieved by co-culture with astrocytes or growth as organoids may better support phenotypic rescue. However, there may also be specific therapeutic windows for particular phenotypes. Our iPSC model system is not ideal for teasing out these differences. Interestingly, *UBE3A* normalization at both 6 and 16 weeks rescued the decrease in spontaneous inhibitory synaptic events and also rescued the increase in spontaneous neuronal firing.

Dup15q is a complicated genetic disorder caused by copy number variation affecting many genes. To begin to dissect the roles of the individual genes, we eliminated the extra chromosome in idic(15) iPSCs to generate the first isogenic human iPSC cell pair. This isogenic pair enabled us to investigate the role of *UBE3A*, a gene thought to play a major role in the disorder, in the development of Dup15q cellular phenotypes. We found that *UBE3A* overexpression is necessary for most of the cellular phenotypes we interrogated. However, some phenotypes, most notably synaptic phenotypes and input resistance, were not completely dependent on *UBE3A* overexpression, suggesting an important role for other genes in the duplicated region. This could include non-imprinted genes as well as paternally expressed genes, as some patients with paternal duplications present with ASD (Al Ageeli et al., 2014), and normalized copy number of *NDN* rescued ASD-like phenotypes, dendritic spine dynamics, and cortical excitatory-inhibitory balance in paternal 15q duplication mice (Tamada et al., 2021). Future studies to identify these additional gene(s) and investigate how excess *UBE3A* and/or other genes cause the neuronal

Figure 6. *UBE3A* overexpression recapitulates intrinsic excitability phenotypes but not synaptic deficits of Dup15q neurons

(A) Experimental design. Neurons differentiated from an iPSC line with a paternal duplication in Chr15 encompassing the *UBE3A* region were treated with 10 μM scramble or *UBE3A-ATS* ASOs at 6 weeks.

(B) qRT-PCR showing relative *UBE3A* mRNA expression in PatDup treated with either scramble (Scr) ASO or *UBE3A-ATS* ASO. ASO treatment was carried out at 6 weeks, and gene expression was analyzed at 8 weeks and 19 weeks *in vitro* (n = 2 biological replicates).

(C) Input resistance obtained using a 10 mV hyperpolarizing step. Unpaired t test.

(D) Left: example inward and outward currents at 19 weeks elicited with a voltage step from −70 to +40 mV. Middle: maximum inward current density. Right: maximum outward current density. Student's t test.

(E) Left: example action potential (AP) traces at 19 weeks elicited by +80 pA current step. Middle: peak AP amplitude. Right: AP width at half of the maximum amplitude. Unpaired t tests.

(F) Left: example AP traces showing the firing rate of 19-week-old cells during a 500 ms current step elicited by +80 pA. Right: maximum AP firing rate. Unpaired t test.

(G) AP firing threshold. Unpaired t test.

(H) Frequency (left) and amplitude (right) of spontaneous excitatory postsynaptic currents (sEPSCs).

(I) Frequency (left) and amplitude (right) of spontaneous inhibitory postsynaptic currents (sIPSCs). Box-and-whisker plots represent the first quartile, median, and third quartile; bars represent 2.5th to 97.5th percentile outliers. *$p < 0.05$ (Mann-Whitney U test). n = 10 cells per group from two independent differentiations.

pathophysiology may open the door for the discovery of new therapeutic approaches and guide research efforts toward creating a more comprehensive animal model that will better encompass Dup15q behavioral and physiological phenotypes.

EXPERIMENTAL PROCEDURES

Resource availability

Corresponding author

Further information and requests for resources and reagents should be directed to and will be fulfilled by the lead contact, Eric S. Levine (eslevine@uchc.edu).

Materials availability

All non-commercially available materials used in this work will be available upon request to the authors.

Data and code availability

This paper reports no original code. No standardized datasets are presented. Original data will be shared by the corresponding author upon request.

iPSC lines and CRISPR-Cas9-mediated genome editing

Studies were carried out using iPSC lines generated from two idic(15) Dup15q patients (idic-1 and idic-2) and one individual with a paternal 15q11-q13 interstitial duplication. The H9 human embryonic stem cell line and an iPSC line from an unaffected individual were used as controls. These lines were previously characterized (Germain et al., 2014; Fink et al., 2021) and are available from the UConn Cell and Genome Engineering Core. To create an isogenic corrected line, we began with an idic-1 clone that had also been transduced with a fluorescent reporter. Next, sgRNAs targeting GOLGA8, SNORD116, and SNORD115 were designed using MIT's CRISPR Design Tool (http://crispr.mit.edu; Table S2) and cloned into pX459v2.0 (Addgene 62988) vector. Briefly, idic-1 iPSCs were pre-treated with ROCK inhibitor before being dissociated into single cells and nucleofected with CRISPRs. iPSCs were then plated onto puromycin-resistant (DR4) irradiated mouse embryonic fibroblasts (irrMEFs) and selected for 48 h with puromycin (0.5–1 μg/mL).

Genomic DNA was isolated from colonies that survived puromycin selection and were screened using qPCR-based TaqMan Copy Number Assays for *UBE3A* and *PML* to identify clones that had lost a 15q11-q13 allele and/or a full chromosome 15 (*UBE3A* Hs03908756_cn; *PML* HS00039647_cn; Life Technologies, Grand Island, NY). The RNase P Copy Number Reference Assay was used in a duplex reaction as an endogenous reference gene to allow quantification of copy number for *UBE3A* and *PML*. *PML* was quantified to exclude clones that had lost an entire chromosome 15, and to increase confidence that the copy number calls for *UBE3A* were not due to PCR artifact. Data analysis was carried out using the CopyCaller version 2.0 software from Applied Biosystems (Life Technologies, Grand Island NY).

Clones with decreased *UBE3A* copy number, but normal *PML* copy number were expanded on irrMEFs and then subjected to quantitative DNA methylation analysis at SNRPN to determine the parent of origin of the remaining 15q11-q13 alleles. One clone showed a reduction of *UBE3A* and 50% methylation at SNRPN, suggesting that it had lost two maternal copies of chromosome 15q11-q13. This clone was subsequently characterized using a cytoSNP array, metaphase karyotyping, confirmatory quantitative DNA methylation analysis, and gene expression analysis. This characterization revealed no other genetic structural variation compared with the parent line. The sequence of TaqMan probe qRT-PCR assays used in the study are provided in Table S4.

Stem cell culture

Mitomycin C-treated mouse embryonic fibroblasts (Millipore, Burlington MA) and human embryonic stem cell (hESC) medium were used to culture iPSCs. hESC medium contained DMEM-F12 (Life Technologies, Carlsbad, CA), 0.1 mM non-essential amino acids, 20% knockout serum replacer, 1 mM L-glutamine, 10 ng mL^{-1} basic fibroblast growth factor , and 0.1 mM 2-mercaptoethanol. A humidified incubator with 5% CO_2 was used to maintain the cells at 37°C. Stem cells were mechanically passaged once per week using a 28G needle, and hESC medium was replaced daily.

Neuronal differentiation and maintenance

Neuronal differentiation was carried out according to established monolayer differentiation protocols with minor modifications (Germain et al., 2014). Briefly, dual-SMAD inhibition using Noggin and SB431542 was carried out for 10 days, neuronal rosettes were passaged on day 14, cells were dissociated using Accutase and replated on day 17, and NPCs (neural progenitor cells) were dissociated and frozen on day 28. NPCs were subsequently thawed and plated on polyornithine/laminin-coated coverslips to perform experiments. Detailed differentiation and maintenance protocols are provided in the supplemental experimental procedures.

Antisense oligonucleotides

UBE3A ASOs and *UBE3A-ATS* ASOs were used to knock down or overexpress *UBE3A*, respectively. Control scramble sequence ASOs were also used. All ASOs were provided by Ionis Pharmaceuticals (Carlsbad, CA) and synthesized as previously described (Meng et al., 2015). ASOs were 20 bp in length with ten DNA nucleotides in the center, a phosphorothioate backbone, and five 2′-*O*-methoxyethyl-modified nucleotides at each end. The ASOs were added directly to the culture media at 10 μM concentration. After 72 h, the media was completely removed and cells were fed with fresh media. iPSC-derived neurons exposed to a single treatment with *UBE3A* ASOs led to sustained mRNA and protein knockdown (Fink et al., 2017; Germain et al., 2021). The sequences of all ASOs used in the study are provided in Table S3.

Electrophysiology

Coverslips were transferred to a recording chamber fixed to an Olympus BX51WI upright microscope stage. Neurons were visualized using a 40x water-immersion lens and identified on the basis of morphology. A continuous flow of oxygenated artificial cerebrospinal fluid (aCSF) containing: 125 mM NaCl, 2.5 mM KCl, 15.0 mM dextrose, 1.25 mM NaH_2PO_4, 2.0 mM $MgCl_2$-$6H_2O$, 25.0 mM $NaHCO_3$, and 2.0 mM $CaCl_2$ was maintained at a rate of 1.5 mL/min. All recordings were done at room temperature. Pipettes with a resistance ranging from 5–8 MΩ were pulled from

borosilicate glass capillaries using Flaming/Brown P-97 micropipette puller and filled with an internal solution containing: 125.0 mM K-gluconate, 4.0 mM KCl, 10.0 mM HEPES, 10.0 mM phosphocreatine, 4.0 mM Na_2-ATP, 0.3 mM Na-GTP, 0.20 mM $CaCl_2$, and 1.0 mM EGTA. Input resistance was monitored throughout the recordings by applying a 10 mV hyperpolarizing step from −70 mV. Neurons were excluded from the analysis if (1) the series resistance exceeded 50 MΩ, (2) the input resistance changed by >15% during the course of experiments, or (3) the input resistance fell below 100 MΩ. Detailed voltage and current-clamp protocols are provided in the supplemental experimental procedures.

Calcium imaging

X-Rhod-1 dye (Thermo Fisher Scientific), reconstituted with DMSO, was added to the cell culture media for a final concentration of 2 μM. Coverslips were incubated with this mixture for 1 h at 37°C then transferred to the recording chamber and perfused with aCSF for 15 min before imaging. Neurons were imaged using a Cairn OptoLED light source system at 594 nM (Texas Red), SM-CCD67 camera at 100 Hz, and Turbo-SM software. Analysis of the data was performed as previously described using Fluorescence Single Neuron and Network Analysis Package (FluoroSNNAP) (Fink et al., 2017). Spontaneous activity was recorded for 15 min from each coverslip.

Immunocytochemistry

Detailed methods are included in the supplemental experimental procedures.

qRT-PCR

Detailed methods are included in the supplemental experimental procedures.

Statistical analysis

Prism software (GraphPad, San Diego CA) was used for all statistical analyses. For normally distributed data, parametric Student's t test or one-way repeated-measures ANOVA and Dunnett's multiple-comparisons tests were used as indicated in the respective graphs. Data are presented as mean ± SEM. For data that are not normally distributed, a non-parametric Mann-Whitney U test was used, and data were represented in box-and-whisker plots representing the median, first, and third quartiles, and error bars representing 2.5th to 97.5th percentile outliers. All statistical significance values of less than 0.05 are represented by an asterisk.

SUPPLEMENTAL INFORMATION

Supplemental information can be found online at https://doi.org/10.1016/j.stemcr.2023.02.002.

AUTHOR CONTRIBUTIONS

M.E., C.C., and D.G. conducted experiments and analyzed data. A.D. and C.S. carried out genome editing to generate the isogenic cell line. T.M.R. designed and optimized experimental procedures. M.E., S.J.C., and E.S.L. designed the project and wrote the manuscript. All authors were involved in the preparation and review of the manuscript and approved the final submitted version.

ACKNOWLEDGMENTS

This work was supported by National Institutes of Health (NIH) grants NS111965 (E.S.L. and S.J.C.) and NS111986 (E.S.L.), the Eagles Autism Foundation (E.S.L.), and the Schlumberger Foundation (M.E.).

CONFLICT OF INTERESTS

S.J.C. is an employee of Roche and shareholder of Ovid Therapeutics. E.S.L. is a member of the scientific advisory board of Kicho.

Received: March 30, 2022
Revised: February 2, 2023
Accepted: February 6, 2023
Published: March 9, 2023

REFERENCES

Adikusuma, F., Williams, N., Grutzner, F., Hughes, J., and Thomas, P. (2017). Targeted deletion of an entire chromosome using CRISPR/Cas9. Mol. Ther. *25*, 1736–1738.

Al Ageeli, E., Drunat, S., Delanoe, C., Perrin, L., Baumann, C., Capri, Y., Fabre-Teste, J., Aboura, A., Dupont, C., Auvin, S., et al. (2014). Duplication of the 15q11-q13 region: clinical and genetic study of 30 new cases. Eur. J. Med. Genet. *57*, 5–14.

Aypar, U., Brodersen, P.R., Lundquist, P.A., Dawson, D.B., Thorland, E.C., and Hoppman, N. (2014). Does parent of origin matter? Methylation studies should be performed on patients with multiple copies of the Prader-Willi/Angelman syndrome critical region. Am. J. Med. Genet. *164A*, 2514–2520.

Chamberlain, S.J., and Lalande, M. (2010). Neurodevelopmental disorders involving genomic imprinting at human chromosome 15q11-q13. Neurobiol. Dis. *39*, 13–20.

Conant, K.D., Finucane, B., Cleary, N., Martin, A., Muss, C., Delany, M., Murphy, E.K., Rabe, O., Luchsinger, K., Spence, S.J., et al. (2014). A survey of seizures and current treatments in 15q duplication syndrome. Epilepsia *55*, 396–402.

Cook, E.H., Jr., Lindgren, V., Leventhal, B.L., Courchesne, R., Lincoln, A., Shulman, C., Lord, C., and Courchesne, E. (1997). Autism or atypical autism in maternally but not paternally derived proximal 15q duplication. Am. J. Hum. Genet. *60*, 928–934.

Copping, N.A., Christian, S.G.B., Ritter, D.J., Islam, M.S., Buscher, N., Zolkowska, D., Pride, M.C., Berg, E.L., LaSalle, J.M., Ellegood, J., et al. (2017). Neuronal overexpression of Ube3a isoform 2 causes behavioral impairments and neuroanatomical pathology relevant to 15q11.2-q13.3 duplication syndrome. Hum. Mol. Genet. *26*, 3995–4010.

DeVos, S.L., and Miller, T.M. (2013). Antisense oligonucleotides: treating neurodegeneration at the level of RNA. Neurotherapeutics *10*, 486–497.

DiStefano, C., Gulsrud, A., Huberty, S., Kasari, C., Cook, E., Reiter, L.T., Thibert, R., and Jeste, S.S. (2016). Identification of a distinct developmental and behavioral profile in children with Dup15q syndrome. J. Neurodev. Disord. *8*, 19.

DiStefano, C., Wilson, R.B., Hyde, C., Cook, E.H., Thibert, R.L., Reiter, L.T., Vogel-Farley, V., Hipp, J., and Jeste, S. (2020). Behavioral

characterization of dup15q syndrome: toward meaningful endpoints for clinical trials. Am. J. Med. Genet. *182*, 71–84.

Fink, J.J., Robinson, T.M., Germain, N.D., Sirois, C.L., Bolduc, K.A., Ward, A.J., Rigo, F., Chamberlain, S.J., and Levine, E.S. (2017). Disrupted neuronal maturation in Angelman syndrome-derived induced pluripotent stem cells. Nat. Commun. *8*, 15038.

Fink, J.J., Schreiner, J.D., Bloom, J.E., James, J., Baker, D.S., Robinson, T.M., Lieberman, R., Loew, L.M., Chamberlain, S.J., and Levine, E.S. (2021). Hyperexcitable phenotypes in induced pluripotent stem cell-derived neurons from patients with 15q11-q13 duplication syndrome, a genetic form of autism. Biol. Psychiatry *90*, 756–765.

Friedman, D., Thaler, A., Thaler, J., Rai, S., Cook, E., Schanen, C., and Devinsky, O. (2016). Mortality in isodicentric chromosome 15 syndrome: the role of SUDEP. Epilepsy Behav. *61*, 1–5.

Germain, N.D., Chen, P.F., Plocik, A.M., Glatt-Deeley, H., Brown, J., Fink, J.J., Bolduc, K.A., Robinson, T.M., Levine, E.S., Reiter, L.T., et al. (2014). Gene expression analysis of human induced pluripotent stem cell-derived neurons carrying copy number variants of chromosome 15q11-q13.1. Mol. Autism. *5*, 44.

Germain, N.D., Gorka, D., Drennan, R., Jafar-nejad, P., Whipple, A., Core, L., Levine, E.S., Rigo, F., and Chamberlain, S.J. (2021). Antisense oligonucleotides targeting UBE3A-ATS restore expression of UBE3A by relieving transcriptional interference. Preprint at bioRxiv. https://doi.org/10.1101/2021.07.09.451826.

Gupta, N., Susa, K., Yoda, Y., Bonventre, J.V., Valerius, M.T., and Morizane, R. (2018). CRISPR/Cas9-based targeted genome editing for the development of monogenic diseases models with human pluripotent stem cells. Curr. Protoc. Stem Cell Biol. *45*, e50.

Hogart, A., Wu, D., LaSalle, J.M., and Schanen, N.C. (2010). The comorbidity of autism with the genomic disorders of chromosome 15q11.2-q13. Neurobiol. Dis. *38*, 181–191.

Huang, L., Kinnucan, E., Wang, G., Beaudenon, S., Howley, P.M., Huibregtse, J.M., and Pavletich, N.P. (1999). Structure of an E6AP-UbcH7 complex: insights into ubiquitination by the E2-E3 enzyme cascade. Science *286*, 1321–1326.

Judson, M.C., Wallace, M.L., Sidorov, M.S., Burette, A.C., Gu, B., van Woerden, G.M., King, I.F., Han, J.E., Zylka, M.J., Elgersma, Y., et al. (2016). GABAergic neuron-specific loss of Ube3a causes angelman syndrome-like EEG abnormalities and enhances seizure susceptibility. Neuron *90*, 56–69.

Kalsner, L., and Chamberlain, S.J. (2015). Prader-willi, angelman, and 15q11-q13 duplication syndromes. Pediatr. Clin. North Am. *62*, 587–606.

Krishnan, V., Stoppel, D.C., Nong, Y., Johnson, M.A., Nadler, M.J.S., Ozkaynak, E., Teng, B.L., Nagakura, I., Mohammad, F., Silva, M.A., et al. (2017). Autism gene Ube3a and seizures impair sociability by repressing VTA Cbln1. Nature *543*, 507–512.

Low, D., and Chen, K.S. (2010). Genome-wide gene expression profiling of the Angelman syndrome mice with Ube3a mutation. Eur. J. Hum. Genet. *18*, 1228–1235.

Mao, R., Jalal, S.M., Snow, K., Michels, V.V., Szabo, S.M., and Babovic-Vuksanovic, D. (2000). Characteristics of two cases with dup(15)(q11.2-q12): one of maternal and one of paternal origin. Genet. Med. *2*, 131–135.

Marini, C., Cecconi, A., Contini, E., Pantaleo, M., Metitieri, T., Guarducci, S., Giglio, S., Guerrini, R., and Genuardi, M. (2013). Clinical and genetic study of a family with a paternally inherited 15q11-q13 duplication. Am. J. Med. Genet. *161A*, 1459–1464.

Meng, L., Ward, A.J., Chun, S., Bennett, C.F., Beaudet, A.L., and Rigo, F. (2015). Towards a therapy for Angelman syndrome by targeting a long non-coding RNA. Nature *518*, 409–412.

Mohandas, T.K., Park, J.P., Spellman, R.A., Filiano, J.J., Mamourian, A.C., Hawk, A.B., Belloni, D.R., Noll, W.W., and Moeschler, J.B. (1999). Paternally derived de novo interstitial duplication of proximal 15q in a patient with developmental delay. Am. J. Med. Genet. *82*, 294–300.

Nakatani, J., Tamada, K., Hatanaka, F., Ise, S., Ohta, H., Inoue, K., Tomonaga, S., Watanabe, Y., Chung, Y.J., Banerjee, R., et al. (2009). Abnormal behavior in a chromosome-engineered mouse model for human 15q11-13 duplication seen in autism. Cell *137*, 1235–1246.

Nawaz, Z., Lonard, D.M., Smith, C.L., Lev-Lehman, E., Tsai, S.Y., Tsai, M.J., and O'Malley, B.W. (1999). The Angelman syndrome-associated protein, E6-AP, is a coactivator for the nuclear hormone receptor superfamily. Mol. Cell Biol. *19*, 1182–1189.

Punt, A.M., Judson, M.C., Sidorov, M.S., Williams, B.N., Johnson, N.S., Belder, S., den Hertog, D., Davis, C.R., Feygin, M.S., Lang, P.F., et al. (2022). Molecular and behavioral consequences of Ube3a gene overdosage in mice. JCI Insight *7*, e158953.

Smith, S.E.P., Zhou, Y.D., Zhang, G., Jin, Z., Stoppel, D.C., and Anderson, M.P. (2011). Increased gene dosage of Ube3a results in autism traits and decreased glutamate synaptic transmission in mice. Sci. Transl. Med. *3*, 103ra97.

Tamada, K., Fukumoto, K., Toya, T., Nakai, N., Awasthi, J.R., Tanaka, S., Okabe, S., Spitz, F., Saitow, F., Suzuki, H., and Takumi, T. (2021). Genetic dissection identifies Necdin as a driver gene in a mouse model of paternal 15q duplications. Nat. Commun. *12*, 4056.

Urraca, N., Cleary, J., Brewer, V., Pivnick, E.K., McVicar, K., Thibert, R.L., Schanen, N.C., Esmer, C., Lamport, D., and Reiter, L.T. (2013). The interstitial duplication 15q11.2-q13 syndrome includes autism, mild facial anomalies and a characteristic EEG signature. Autism Res. *6*, 268–279.

Wang, H., Yang, H., Shivalila, C.S., Dawlaty, M.M., Cheng, A.W., Zhang, F., and Jaenisch, R. (2013). One-step generation of mice carrying mutations in multiple genes by CRISPR/Cas-mediated genome engineering. Cell *153*, 910–918.

Xiao, A., Wang, Z., Hu, Y., Wu, Y., Luo, Z., Yang, Z., Zu, Y., Li, W., Huang, P., Tong, X., et al. (2013). Chromosomal deletions and inversions mediated by TALENs and CRISPR/Cas in zebrafish. Nucleic Acids Res. *41*, e141.

Zuo, E., Huo, X., Yao, X., Hu, X., Sun, Y., Yin, J., He, B., Wang, X., Shi, L., Ping, J., et al. (2017). CRISPR/Cas9-mediated targeted chromosome elimination. Genome Biol. *18*, 224.